Optimisation of Manufacturing Parameters and Morphology-Based Numerical Analysis of Nanocomposites

D. Bhattacharyya
Centre for Advanced Composite Materials
The University of Auckland, Private Bag 92019
Auckland, New Zealand

Y. Dong
Department of Mechanical Engineering
Curtin University of Technology, GPO Box U1987
Perth, WA 6845, Australia

Abstract

In recent years, the usage of polymer nanocomposites has been increasing rapidly. However, although their functional properties are superior, often the relevant mechanical properties do not give sufficient consistency to satisfy the expectations of the users. In most cases, the property variations come from the manufacturing methods and the lack of knowledge of the individual parameter's effects. The present paper describes a comprehensive approach towards determining the optimised formulation, melt compounding of the nanomaterials and numerical simulation which is based on the microscopic image processing of real morphological structures of polypropylene (PP)/clay nanocomposites. In this study, first of all, PP/clay nanocomposites are investigated with respect to their manufacturing and resulting morphology. The manufacturing parameter optimisation is carried out by implementing the methodology of Taguchi design of experiments (DoE). Clay type and content, compatibiliser content and PP type are varied to produce the combinations of factors that maximise (not simultaneously) the tensile/ flexural moduli and strengths as well as the impact strengths of prepared nanocomposites. A global sub-optimised combination is found for producing nanocomposites that possess good individual mechanical properties. Subsequently, object-oriented finite element (OOF) technique is used to incorporate the acquired morphological images of final optimised nanocomposites into two-dimensional finite element modelling. An understanding of the overall material behaviour is developed through the combination of real data from micro/nanostructures and the fundamental material characteristics of the constitutive phases. Captured morphological images, using either scanning electron microscopy (SEM) or transmission electron microscopy (TEM), are utilised to generate the geometric information regarding the nano/microstructures. The material properties, on the other hand, are obtained from conducted tests and published literature. The numerical results predicting the elastic moduli of polypropylene/clay nanocomposites are compared with the experimental data and the available composites theoretical models. Very good agreement has been shown to exist establishing the viability of this kind of numerical approach.

Introduction

The success of using layered silicates as nanofillers in polymer nanocomposites (e.g. polyamide/clay nanocomposites) has greatly motivated researchers and engineers due to the materials' capability of accomplishing the property enhancements such as high stiffness, light weight and good heat resistance at a low clay content ($\leq$ 5 wt%). Furthermore, the recent focus has been extended to low cost polyolefin-based nanocomposites like using polypropylene (PP) as the polymer matrix. PP, as a commonly used commodity polymer, has a variety of material merits including low density, high thermal stability, excellent processibility as well as wide usages in automotive and packaging industries. Nevertheless, its low modulus relative to engineering polymers (e.g. nylon 6) might limit the material selection to meet the requirements of end users. This disadvantage can be potentially alleviated by the additional good clay dispersion. PP/clay nanocomposites, prepared by either conventional intensive shear mixing or twin screw extrusion have been successfully produced with partially intercalated/exfoliated structures [1-5]. The major problem to address originates from very low interactions between the non-polar hydrophobic PP and hydrophilic clay to hinder the early stage of effective intercalation. The direct way to increase the compatibility between the PP matrix and clay lies in blending PP with compatibilisers, such as maleic anhydride grafted PP (MAPP) oligomer, to enlarge the interlayer spacing and facilitate the penetration of clay platelets. Although the complete

clay exfoliation as the favourable morphology of PP/clay nanocomposites has not been experimentally achieved so far, the enhancements of stiffness and strength at a low clay content are still very attractive from the industrial point of view. Previous work [6-9] done by the other researchers reported the inconsistencies of modulus and strength increases possibly due to the complex influence of the material selection and the melt processing methods. Those contradictory results necessitate a systematic study in the formulation and fabrication of such nanocomposites in place of the "trial and error" experimental method in the common polymer blending approach.

On the other hand, despite tremendous opportunities offered by dispersing nanofillers into the continuous polymer matrix in a nanocomposite system, an effective multi-scale numerical approach to predict the overall material behaviour from the complex constituents is still at an infant stage. In particular, the modulus prediction of nanocomposites has been initiated using three widely accepted approaches comprising composites theoretical models, finite element analysis (FEA) and molecular dynamic (MD) simulation. Halpin-Tsai and Mori-Tanaka models [10, 11] are very simple and rough closed-form analytical solutions to originally predict the material properties of short-fibre composites. Great efforts have been made with some success using those models to estimate the elastic modulus [12-15], thermo-mechanical properties [12] and the reinforcement efficiency of polymer/clay nanocomposites [15]. As far as the numerical simulation is concerned, MD simulation considers far more accurate model development of thermodynamics and kinetics of formation, based on the discrete atom or molecule as the fundamental unit. It provides a very advanced approach down to the nanoscale level to predict their relevant molecular interactions [16-18], interlayer spacing [19-21], binding energy [19-22] and elastic properties [17]. However, this approach solely concentrates on the local molecular/atomic interactions and hierarchical structures and behaviour, which might be constrained by scaling up the integrated lengths or huge time scales to globally characterise the structures of nanocomposites. The applicability of continuum mechanics using FEA has also been subjected to great attention by applying the integrated representative volume elements (RVE) with a nanometric second phase [14, 23, 24]. The general use of microstructures of composite materials by either well-aligned RVE [23, 24] or randomly distributed RVE with Monte Carlo method [14] still cannot conform to the actual complicated and highly heterogeneous nanocomposite morphology. As a result, the lack of a fine detailed structural interpretation necessitates the object-oriented finite element (OOF) analysis [25-27] to deal with a small-scaled and disordered heterogeneous material system. OOF analysis is quite a novel numerical approach to incorporate morphological images, acquired from scanning electron microscopy (SEM) or transmission electron microscopy (TEM), into 2-D finite element modelling by mapping the computational grid, as illustrated in Fig.1. The advantage of OOF technique is to combine the data in the real form of micro/nanostructures such as particle size, shape, spatial position and real orientation with fundamental material parameters including elastic modulus, Poisson's ratio, coefficient of thermal expansion of constitutive phases to understand the overall material behaviour. Although OOF is temporarily limited to the calculations of elasticity and thermal conductivity in 2-D microstructures, it has also given very promising results in analysing stress transfer [28], fracture mechanisms [29-31], crack propagations [32], residual thermal stresses [33, 34] and thermal conductivities [35] of heterogeneous materials. More recently, OOF modelling has also been employed in predicting the elastic moduli of nanocomposites, in reasonable agreement with experimental data and theoretical analyses of Halpin-Tsai and Lewis-Nielsen models [36-38].

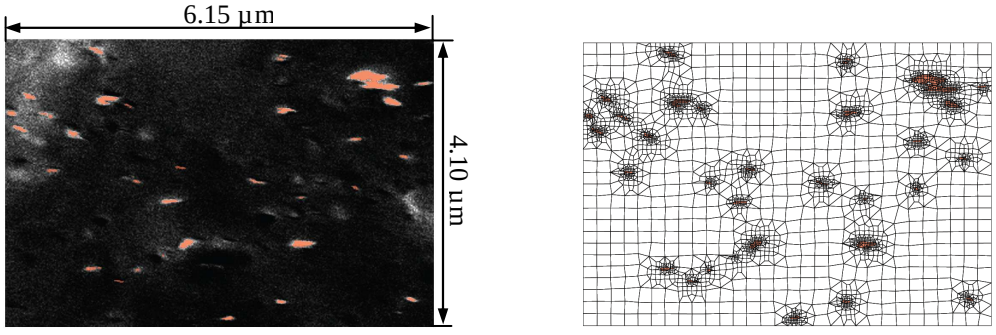

Fig.1 A micro/nanostructure based OOF model example of PP/clay nanocomposites: (a) SEM micrograph and (b) finite element mesh [7].

The purpose of this paper is to develop a systematic approach for determining the preferred material formulations and manufacturing procedures using Taguchi design of experiments, characterising the nanocomposite materials, predicting the mechanical properties of PP/clay nanocomposites and evaluating the particle distribution effects on the deformation mechanisms by OOF modelling under linear elastic conditions. The results are then compared with the conventional composite theories in order to understand the micro/nanostructure-mechanical property relationship of tailored PP/clay nanocomposites.

Experimental Details

Material Formulations

The initial material formulations were statistically determined by using well-known Taguchi design of experiments (DoE) [39, 40], which could easily detect the most significant factors for maximising the mechanical properties of nanocomposites and work out their ultimate preferred formulations in a limited number of trials. The layered silicates used in this study were three types of NANOLIN™ organoclay denoted as DK1N, DK2 and DK4, which were obtained from Zhejiang Fenghong Clay Chemicals Co., Ltd, China. They were modified by different levels of cation exchange reaction with octadecylammonium salt [41] to broaden their interlayer spacings (d_{001}=2.29, 2.25 and 3.56 nm, respectively). Three grades of commercially available polypropylene (PP) with the various melt flow indices (MFI), referred to as PP-Co M710 (MFI= 0.6 g/10 min), PP-Hom Y130 (MFI=4.0 g/10 min) and PP-Hom H380F (MFI=25 g/10 min), were also provided by Clariant (New Zealand) Ltd. PP-Co M710 is a high impact PP copolymer with ethylene content of 6 wt%. Maleic anhydride grafted PP (MAPP) Exxelor™ PO1020 (MA content: 0.5-1 wt%, MFI=~430 g/10 min) was selected as the compatibiliser from ExxonMobil Chemical (Germany). Table 1 shows the factors and levels in the nine trails of the DoE work, resulting in a typical three-level four factors L_9 Taguchi DoE layout as illustrated in Table 2. For simplicity, all four factors were assumed to be independent of one another, thus neglecting the factorial interactions.

Table 1 Four factors and three levels used in L_9 DoE layout

Factor	Level		
	1	2	3
A: Clay type	DK1N	DK2	DK4
B: Clay content (wt%)	3	5	10
C: MAPP content (wt%)	5	10	20
D: PP type	PP-Co M710	PP-Hom Y130	PP-Hom H380F

Table 2 L_9 DoE layout for the fabrication of PP/clay nanocomposites

Trial number	Symbol	Clay type	Clay content (wt%)	MAPP content (wt%)	PP type
1	RR1: DK1N/MAPP/Y130 (5/10/85)*	DK1N	5	10	PP-Hom Y130
2	RR2: DK4/MAPP/Y130 (3/20/77)	DK4	3	20	PP-Hom Y130
3	RR3: DK2/MAPP/Y130 (10/5/85)	DK2	10	5	PP-Hom Y130
4	RR4: DK1N/MAPP/M710 (3/5/92)	DK1N	3	5	PP-Co M710
5	RR5: DK2/MAPP/H380F (3/10/87)	DK2	3	10	PP-Hom H380F
6	RR6: DK2/MAPP/M710 (5/20/75)	DK2	5	20	PP-Co M710
7	RR7: DK4/MAPP/M710 (10/10/80)	DK4	10	10	PP-Co M710
8	RR8: K1N/MAPP/H380F (10/20/70)	DK1N	10	20	PP-Hom H380F
9	RR9: DK4/MAPP/H380F (5/5/90)	DK4	5	5	PP-Hom H380F

*Note: * Figures in parentheses (e.g. 5/10/85) indicate the contents (wt%) of organoclay, MAPP and PP in nanocomposites.*

Sample Preparation

PP/clay nanocomposites were prepared by melt compounding PP and MAPP pellets with downstream feeding of clay powders using a co-rotating intermesh twin screw extruder DSE20 (D=20 mm, L:D=40, BRABENDER® OHG, Germany) at 200 rpm and a temperature profile of 185-210°C. The initial nanocomposite batches were then recompounded at 100 rpm in the same conditions to extend the residence time. PP and initial prepared nanocomposite pellets were both fed at 3.0 kg/hr. The final dried nanocomposite pellets were further injection moulded to prepare the mechanical testing samples using a BOY 50A machine at 190-210°C with the die temperature of 25°C and injection pressure at 60-80 bars. More details of such material processing method were elaborated in the earlier literature [42].

Structural and Mechanical Characterisation

The morphology of nanocomposites used in this study was characterised using a Philips CM12 transmission electron microscope at an accelerating voltage of 120 kV. Ultra thin film samples (nominal thickness: 70 nm) were cryosectioned in a longitudinal melt flow direction using a Hitachi S-4700 ultramicrotome at -80 °C.

Mechanical testing was carried out to determine the tensile, flexural and impact properties of PP/clay nanocomposites according to ASTM D638, D790 and D6110, respectively. Tensile and flexural tests were conducted on a universal tensile machine (Instron® 1185) and charpy impact tests were performed on a RESIL® 25 pendulum impact testing apparatus. All the test samples were placed in a vacuum desiccator for over 24 hrs prior to the mechanical testing. The final reported results were based on the average data of five samples with calculated standard deviations.

Results and Discussion

Evaluation of Significant Factors

In order to identify the significant factors to maximise the mechanical properties of PP/clay nanocomposites, a "larger-the-better" characteristic formula was employed, which can be shown as

$$S/N = -10\log\left(\frac{1}{n}\sum_{i=1}^{n}\frac{1}{y_i^2}\right) \quad (1)$$

where *S/N* is the signal-to-noise ratio, *n* is the number of samples in each trial and *y* is the measured response value, namely the normalised moduli or strengths over those of corresponding neat PP.

In addition, a special Pareto Analysis of Variance (ANOVA) technique [39], as a quick and easy approach to analyse the results of parameter design without the requirement of ANOVA table and F-tests, was implemented to examine the determined mechanical properties [42] of formulated nanocomposites listed in Table 2. The general criterion to determine the significant factors in this study was based upon the derived cumulative contribution percentage of about 90% along with the technical and economic considerations for non-significant factors.

The Pareto ANOVA diagrams for each of mechanical parameters are exhibited in Fig. 2. Evidently, PP type (factor D) and clay content (factor B) are regarded as two significant factors with the contribution percentages of 60% and 33%, respectively while clay type (factor A) and MAPP content (factor C) show trivial influence with the sum of the contribution percentages being less than 10%, Fig.2(a). The Pareto ANOVA diagram for the enhancement of tensile strength, as shown in Fig. 2(b), indicates a very similar trend apart from the addition of clay type as the third significant factor. For the

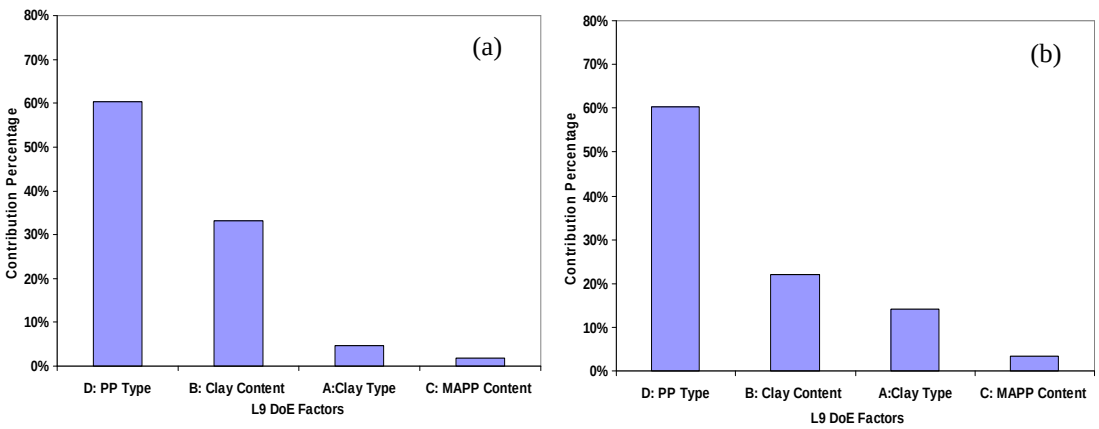

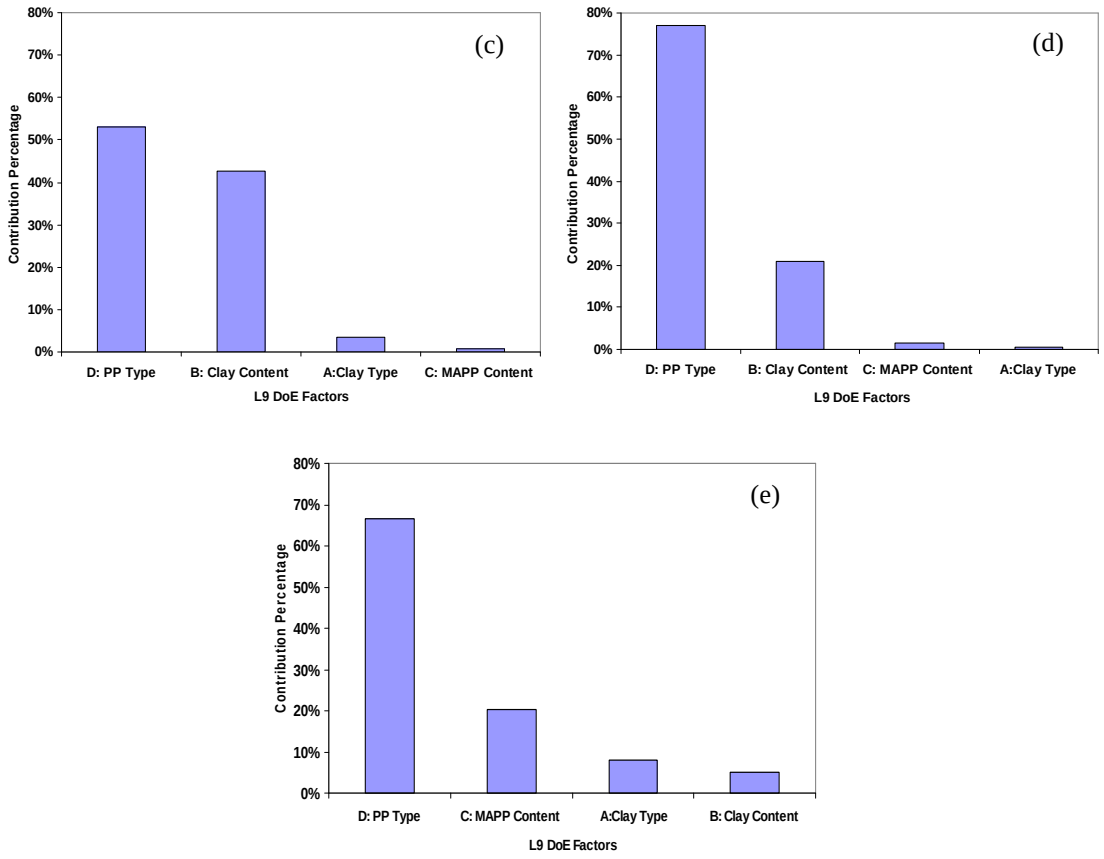

Fig.2 Pareto ANOVA analysis for the enhancement of mechanical parameters of PP/clay nanocomposites: (a) tensile modulus, (b) tensile strength at yield, (c) flexural modulus, (d) flexural strength and (e) charpy impact strength.

flexural properties, the increases of flexural modulus and strength are attributed to the strong effects of PP type (contribution percentages: 53% and 77%) and clay content (contribution percentage: 43% and 21%) correspondingly, Figs. 2(c) and (d). The impact strength, on the other hand, is most likely affected by PP type, MAPP content and clay type (contribution percentages: 67%, 20% and 8%, respectively). Conversely, MAPP content as a second significant factor plays a more important role in the impact properties as compared to tensile and flexural properties.

Determination of Preferred Formulations

It is well understood for the "larger-the-better" characteristics in Taguchi DoE method that the higher the sum of *S/N* ratio is, the better is the response for the factorial effects. Consequently, the sum of *S/N* ratio diagrams are also plotted in Fig. 3 to determine the best combination of factors to enhance each of mechanical parameters along with the respective compositions and estimates of error variance, as listed in Table 3.

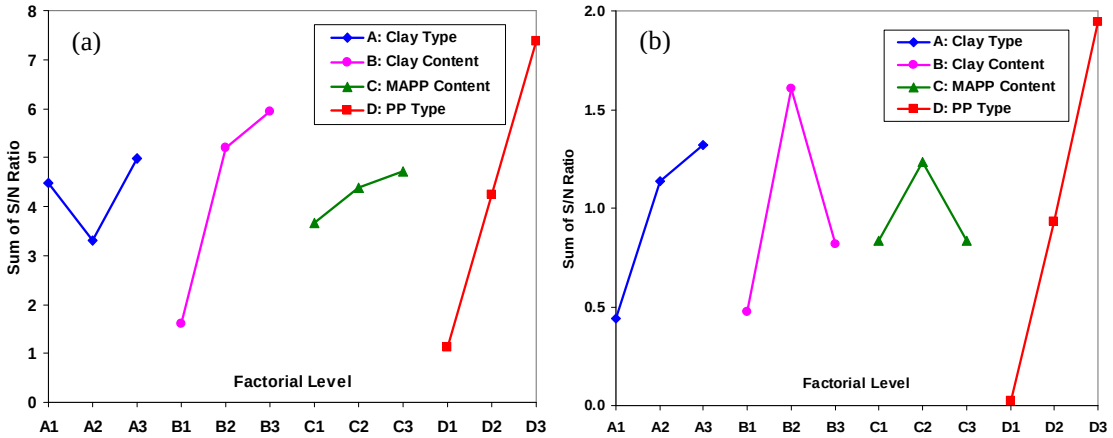

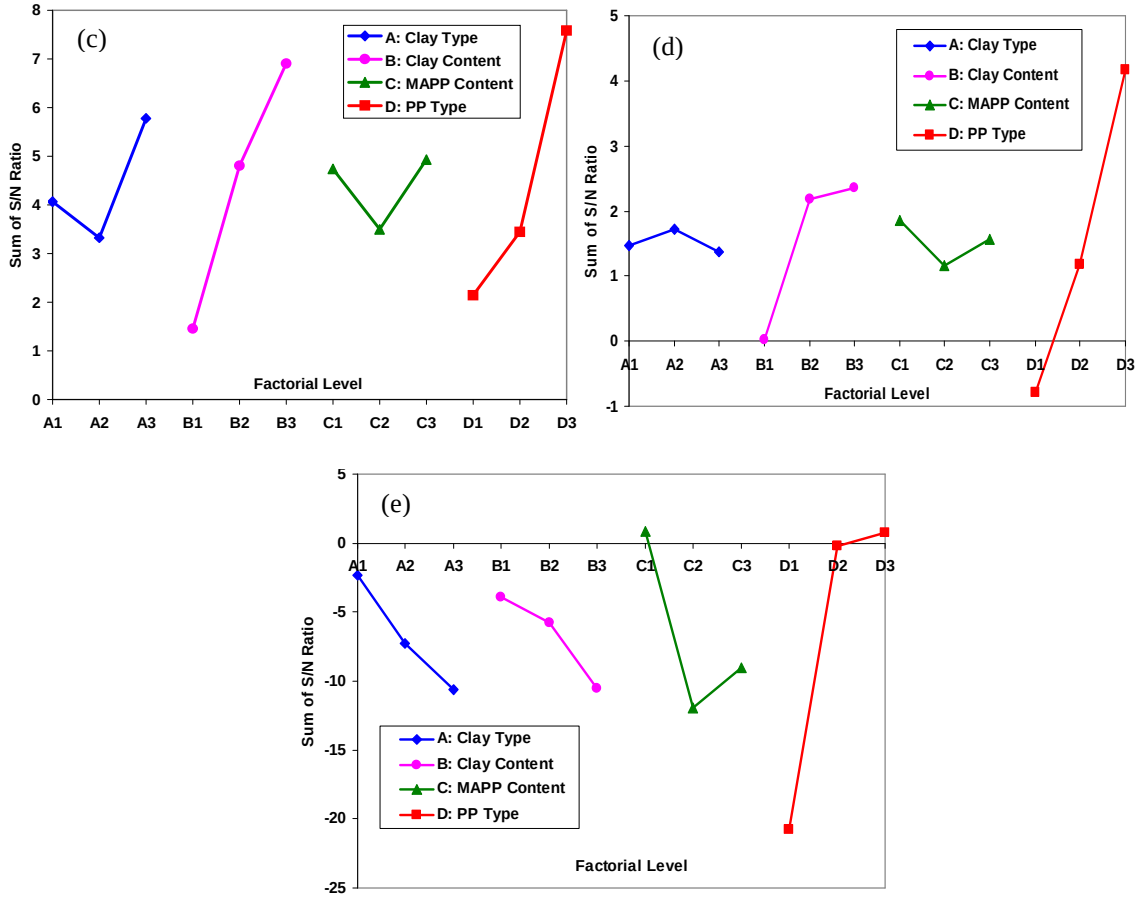

Fig.3 Sum of *S/N* ratio diagrams for the enhancement of mechanical parameters of PP/clay nanocomposites: (a) tensile modulus, (b) tensile strength at yield, (c) flexural modulus, (d) flexural strength and (e) charpy impact strength.

Table 3 Summary of preferred formulations for improving the mechanical properties of PP/clay nanocomposites

	Larger-the-better L_9 DoE response (Normalised)	Preferred factorial level combination	Composition (wt%)	Estimate of error variance
Tensile properties	Tensile modulus	$A_3B_3C_3D_3$	DK4/MAPP/H380F (10/20/70)	0.35
	Tensile strength	$A_3B_2C_2D_3$	DK4/MAPP/H380F (5/10/85)	0.04
Flexural properties	Flexural modulus	$A_3B_3C_3D_3$	DK4/MAPP/H380F (10/20/70)	0.31
	Flexural strength	$A_2B_3C_1D_3$	DK2/MAPP/H380F (10/5/85)	0.05
Impact properties	Impact strength	$A_1B_1C_1D_3$	DK1N/MAPP/H380F (3/5/92)	9.70

This study has solely concentrated on the maximisation of individual mechanical properties of PP/clay nanocomposites due to the difficult processing for the global property enhancement, resulting from some contradictory effects. Thus, a good balance has to be made while increasing the tensile/flexural properties without greatly sacrificing the impact strength. Since DoE results show some significant effects of PP type and clay content on the property enhancement, particularly with PP-Hom H380F as the best performing PP grade, the final optimised formulation was based on using PP-Hom H380F, MAPP and DK4 clay of 3 wt%, 5 wt%, 8 wt% and 10 wt% (weight ratio of MAPP: clay, WR=2:1), which was subjected to the identical sample preparation conditions.

Mechanical Properties of Optimised Nanocomposites

Mechanical properties of final optimised formulation are depicted in Fig.4 compared to those of neat PP-Hom H380F. The addition of clay particles has been proven to yield the overall property enhancements in the presence of MAPP as the compatibliser. Both tensile and flexural moduli demonstrate the better improvements in a relatively monotonic manner with increasing the clay content. At the clay content of 10 wt%, the tensile and flexural moduli have been enhanced by 41% and 61%, respectively. The strengths are also increased up to 16% (tensile) and 22% (flexural), but beyond the threshold of 3 wt% clay, they more or less level off regardless of the clay content. More surprisingly, the impact strength achieves a 50% improvement at the clay content of 3 wt%, after which it declines, reaching the value of neat PP for 10 wt% filled nanocomposites. The enhancement of mechanical properties can be attributed to the good clay dispersion containing the partially exfoliated and intercalated structures [43].

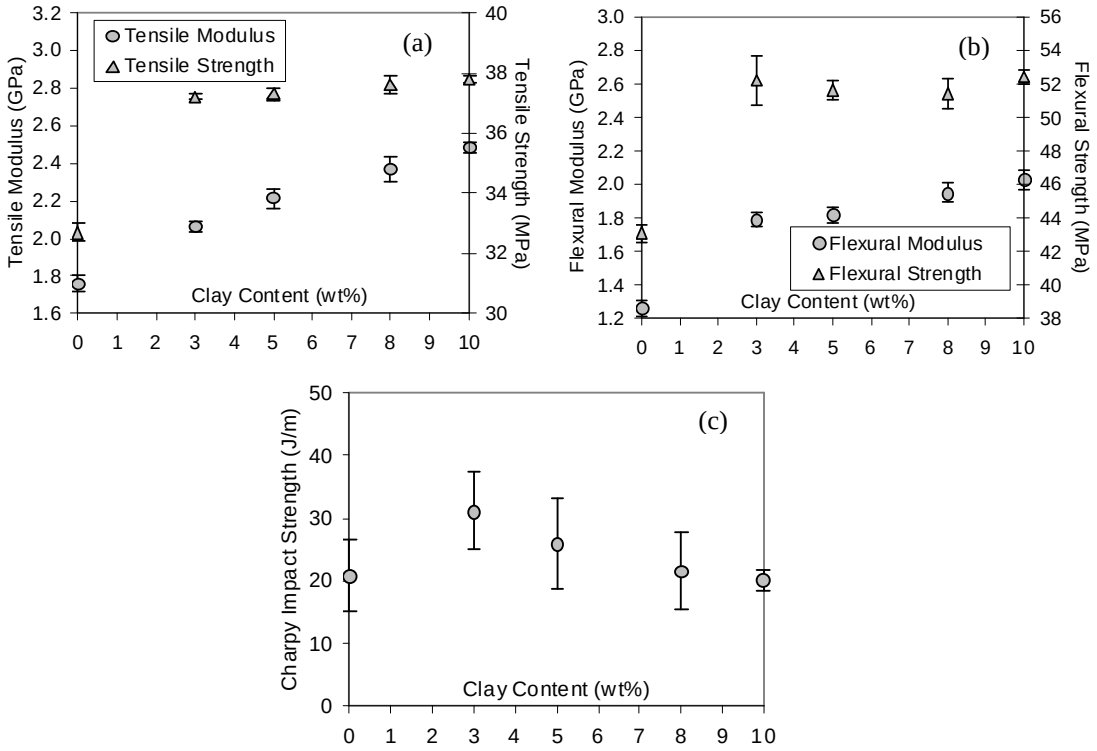

Fig.4 Mechanical properties of optimised PP/clay nanocomposites (weight ratio WR=2:1): (a) tensile properties, (b) flexural properties and (c) impact strength.

Modelling of Elastic Modulus

Composites Theoretical Models

For conventional composite systems, a series of micromechanical models [44] have been developed to handle the factorial effects of filler geometry, content and orientation and the property ratio of filler and matrix on the reinforcement and mechanical properties of composites. Furthermore, the simplified geometry for each constituent and the assumption of perfect bonding interfaces, though not accurate, have been widely admitted by the material manufacturers and engineers to predict the composite stiffness.

Halpin-Tsai model [10] is a well-known composite theory in the fibre composites industry to predict elastic moduli of unidirectional composites as the functions of filler volume fraction and aspect ratio. In this model, filler geometries can be varied including discontinuous reinforcements such as fibre-like or flake-like fillers. The longitudinal and transverse moduli E_{11} and E_{22} of a composite material in Halpin-Tsai model are generally expressed as

$$\frac{E_c}{E_m} = \frac{1+\zeta\eta\phi_f}{1-\eta\phi_f} \tag{2}$$

$$\eta = \frac{\frac{E_f}{E_m} - 1}{\frac{E_f}{E_m} + \zeta} \tag{3}$$

where E_c, E_f, E_m are Young's moduli of composites, fillers and the polymer matrix, respectively. ϕ_f is the filler volume fraction and ζ is a shape parameter depending on the filler geometry and loading direction. ζ=2(L/d) for fibres or 2(L/t) for disk-like platelets when calculating the longitudinal elastic modulus E_{11}, whereas, as an approximation, ζ=2 for transverse elastic modulus E_{22} due to its relative insensitivity to fibre aspect ratio. L, d, t, are the length, diameter and thickness of dispersed fillers, respectively.

Hui-Shia model [45] is developed to predict the elastic moduli of composites including unidirectional aligned platelets with the simple assumption of perfect interfacial bonding between the polymer matrix and platelets, which is given by

Longitudinal elastic modulus (E_{11})

$$\frac{E_c}{E_m}\frac{E_{11}}{E_m} = \frac{1}{1 - \frac{\phi_f}{4}\left[\frac{1}{\xi} + \frac{3}{\xi + \Lambda}\right]} \tag{4}$$

Transverse elastic modulus (E_{22})

$$\frac{E_{22}}{E_m} = \frac{1}{1 - \frac{\phi_f}{\xi}} \tag{5}$$

with
$$\xi = \phi_f + \frac{E_m}{E_f - E_m} + 3(1 - \phi_f)\left[\frac{(1-g)\alpha^2 - \frac{g}{2}}{\alpha^2 - 1}\right] \quad \text{and} \quad g = \frac{\pi}{2}\alpha \tag{6}$$

$$\Lambda = (1 - \phi_f)\left[\frac{3(\alpha^2 + 0.25)g - 2\alpha^2}{\alpha^2 - 1}\right] \tag{7}$$

where $\alpha = t/L$ for disk-like platelets ($\alpha \leq 0.1$).

More importantly, clay platelets in nanocomposites inevitably contain some degree of misalignment and random orientation while in the conventional composite theories, unidirectionally aligned fillers are normally assumed for simplicity. In the case of completely random orientation in all three orthogonal directions, the approximation equations for fibre and platelet reinforced composites moduli $E_{ran\text{-}3D}$ based on the laminate theory [46, 47] are derived as

$$E_{ran-3D}^{fibres} = 0.184 E_{//} + 0.816 E_{\perp} \tag{8}$$

$$E_{ran-3D}^{platelets} = 0.49 E_{//} + 0.51 E_{\perp} \tag{9}$$

where $E_{//}$ and $E_{\perp}$ are the composite moduli in the directions parallel and perpendicular to the major axis of fillers, respectively. Laminate model provides the insight to predict the elastic moduli of nanocompsites with random-oriented clay platelets resembling the real morphological structures.

OOF Modelling

The addition of a small amount of clay particles as rigid nanofillers can significantly enhance the mechanical properties of PP/clay nanocomposites, especially the elastic modulus. Computational models were established using an object-oriented finite element (OOF) code, OOF 2.0.4 [26], developed by the National Institute of Standards and Technology (NIST), USA, to predict their elastic moduli at various clay contents. OOF 2.0.4 was installed in a Fedora Red Hat Core 4 Linux system. The finite element analysis was conducted on a Dell INSPIRON™ 8600 laptop with the Windows XP and Linux dual boot system using 1.6 GHz processors and 2 GB RAM.

Initially, a representative region of interest in Fig. 5(a) was selected from a typical TEM micrograph for 5 wt% filled nanocomposites and then the image segmentation using the pixel selection tool was

employed to assign the material properties of clay particles and the PP matrix, Fig. 5(b). The 2-D finite element mesh was subsequently created based on OOF skeleton to display all the details of micro/nanostructures of clay platelets with the actual size and shape, orientation and spatial position under an adaptive mesh refinement scheme, Fig. 5(c). Both clay particles and the PP matrix were assumed to be isotropic linear elastic materials with the perfect interfacial bonding between the two constituents. The material properties of the constituents used for this study are listed in Table 4, which only consider the simple case of "ideally isotropic homogenised particles" [12, 14, 43, 48] for the intercalated clay platelets to calculate the clay elastic modulus and Poisson's ratio. To define the boundary conditions, as depicted in Fig. 5(c), both x and y displacements U_x, U_y on the left boundary were set to zero (i.e. fully constrained) and U_x on the right boundary is equivalent to 0.05% and 0.25% elastic strains, respectively. The effective elastic modulus of nanocomposites is calculated from the tensile stress resulting from the sum of forces applied on the right boundary. Unit thickness and plane stress conditions are assumed throughout the entire OOF modelling work.

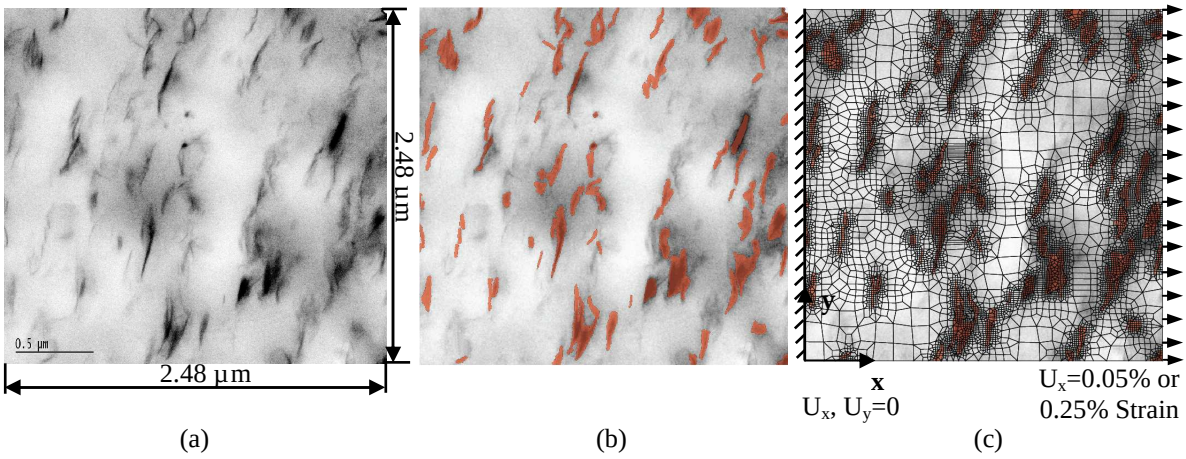

Fig. 5 OOF modelling procedure based on optimised 5 wt% filled PP/clay nanocomposites (WR=2:1): (a) original representative region of interest from a TEM image, (b) pixel selection in the image segmentation and (c) finite element mesh.

Table 4 Constituent properties of PP/clay nanocomposites

	PP matrix	Clay particles	References
Young's modulus (GPa)	1.76[a]	48.3[b]	[a] Experimental data; [b] Calculated on average based on measured d_{001} from [43]
Poisson's ratio	0.35[c]	0.26[d]	[c] [12] and [d][48]
Density (g/cm^3)	0.9	1.8	Material data sheet

Since the orientation of clay particles has a very significant influence on the elastic modulus apart from their aspect ratio and shape parameter [12, 49], OOF modelling results are compared with the experimental data of optimised PP/clay nanocomposites (WR=2:1) and typical Halpin-Tsai and Hui-Shia models with both unidirectional platelet alignment and 3-D random platelet orientation, Fig. 6. Apparently, the modelling results well capture the linear increasing trend of elastic modulus with increasing the clay content, in good accordance with the experimental data though subjected to the slight overestimation. Such discrepancy can be associated with neglect of the compatibiliser and interphase properties as well as the artefacts and phase distinction problem in the imaging analysis. Moreover, it also lies in the simple assumption of perfect bonding condition at the interface, which might not be the case for PP/clay nanocomposites since polyolefin nanocomposites really lack this strong adhesion with only weak van der Waals forces existing in the clay interlayers [50]. On the other hand, due to the presence of prevalent stacks of intercalated platelets within the PP matrix, the experimental data have also fitted composites theoretical models at various clay aspect ratios (L/t= 5~80). It is worth noting that the unidirectional alignment state depends on the theoretical calculations of unmodified Halpin-Tsai and Hui-Shia models in Eqs. 2 and 4, respectively while 3-D random orientation state is on the basis of Halpin-Tsai laminate hybrid and Hui-Shia laminate hybrid models

obtained from Eqs. 2, 4, 5 and 9. As clearly seen in Figs. 6(b) and (d), at a fixed aspect ratio, each curve for the random orientation lies below the corresponding one for the unidirectional alignment, Figs. 6(a) and (c). This is because of the practical standpoint in conventional composite theory that deviations from unidirectional reinforcements inevitably lead to the sizeable reductions in composite stiffness, the extent of which can be dependent on the filler shape [12]. Such modulus reduction phenomenon due to the different filler orientation states becomes more pronounced for Halpin-Tsai laminate hybrid model in comparison to the unmodified Halpin-Tsai model which mainly deals with discontinuous fibre-like fillers, Figs. 6(a) and (b). Nevertheless, Hui-Shia laminate hybrid model demonstrates less modulus reduction as compared to unmodified Hui-Shia model for the disk-like platelet filler geometry with the biaxial reinforcement, Figs. 6(c) and (d). It is clearly pointed out that platelets do not tend to be as sensitive as fibres to the orientation states, which can benefit the nanocomposite system requiring an effective multi-directional reinforcement.

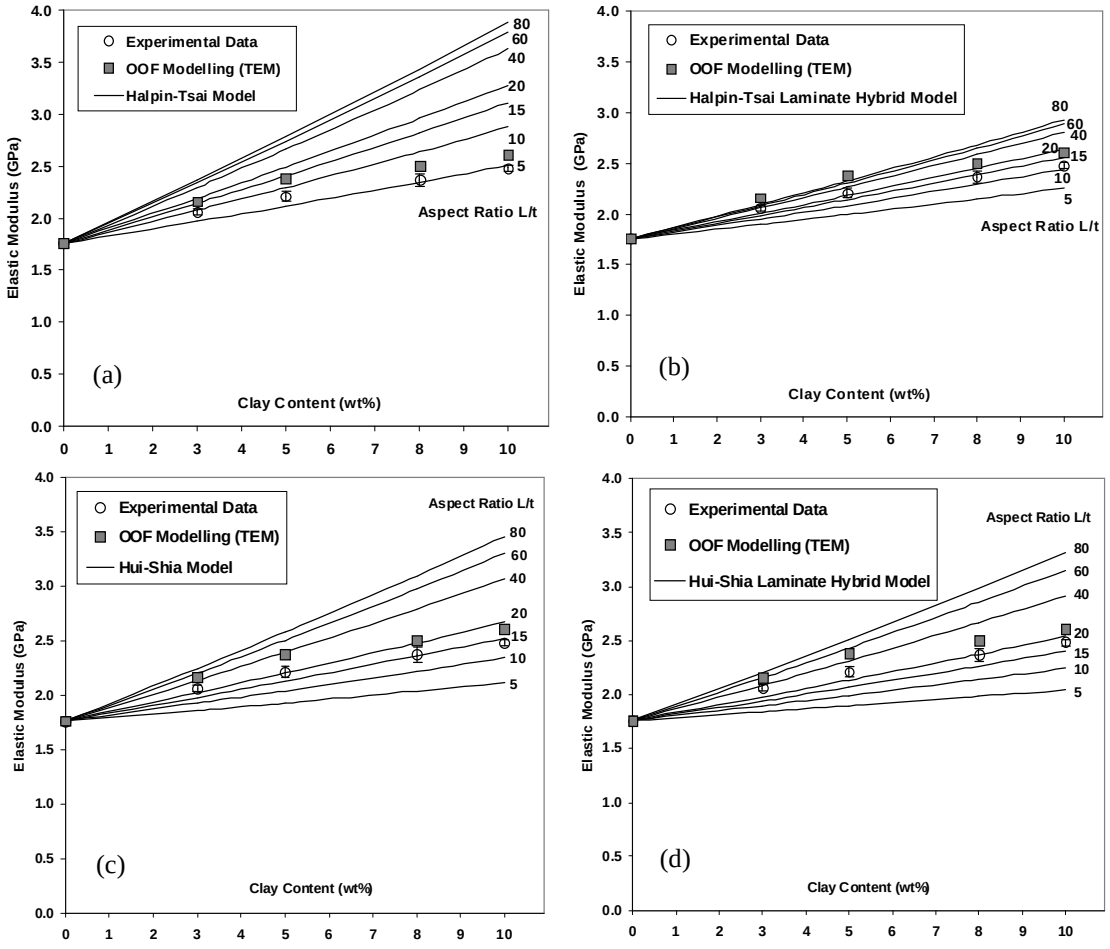

Fig. 6 Comparisons of experimental data, OOF modelling (TEM) results and composites theoretical models: (a) Halpin-Tsai model, (b) Halpin-Tsai laminate hybrid model, (c) Hui-Shia model and (d) Hui-Shia laminate hybrid model for optimised PP/clay nanocomposites (WR=2:1).

The effect of clay dispersion for optimised PP/clay nanocomposites (WR=2:1) has also been investigated from the uniaxial stress contours (σ_{xx}) subjected to 0.25% elastic strain, Fig. 7. As expected, the tensile stresses become much lower in the PP matrix region free of clay particles while the higher stresses are often visible around the interfacial area between clay particles and the PP matrix. It is implied that the interface in nanocomposites plays an important role in the effective load transfer from the matrix to the fillers. Furthermore, increasing the clay content from 3 to 10 wt% can also lead to the stress enhancement on the PP matrix owing to the more frequent particle-to-particle contact when the number of clay particles increases (i.e. decreasing the interparticle spacing). The stress intensification phenomenon becomes very manifest at the sharp edges of clay particles, acting as the stress concentration sites, especially where the clay platelets are tailored to be well-aligned with the loading direction. Similarly, the localised high stress concentration has also been found in the regions

with increasing number of clay particles to contact, which appears to be more pronounced at a higher clay content (8-10 wt%), Figs. 7(c) and (d). The orientation state of clay particles, on the other hand, can also substantially influence the local stresses in a unidirectional tensile mode. As clearly seen in Region A, Fig. 7(a), clay particles with a more favourable alignment along the loading direction undergo higher stresses compared to the particles that are almost perpendicular to the applied load in Region B. This finding also supports the key point in the general composite theories that the variations of composite strength and modulus along the longitudinal and transverse directions are due to the preferential orientation of the fillers. Hence, good alignment of clay particles associated with high aspect ratios within the PP matrix should be quite vital for the effective stress transfer in a nanocomposite system, which is diminished from a practical point of view in the real morphology of nanocomposites owing to various degrees of the random orientation of clay particles. The high localised stress field around clay particles obviously induces the possibility of nanocomposite failure and damage, especially at the higher clay content, resulting from the clay particle clustering and contact increment.

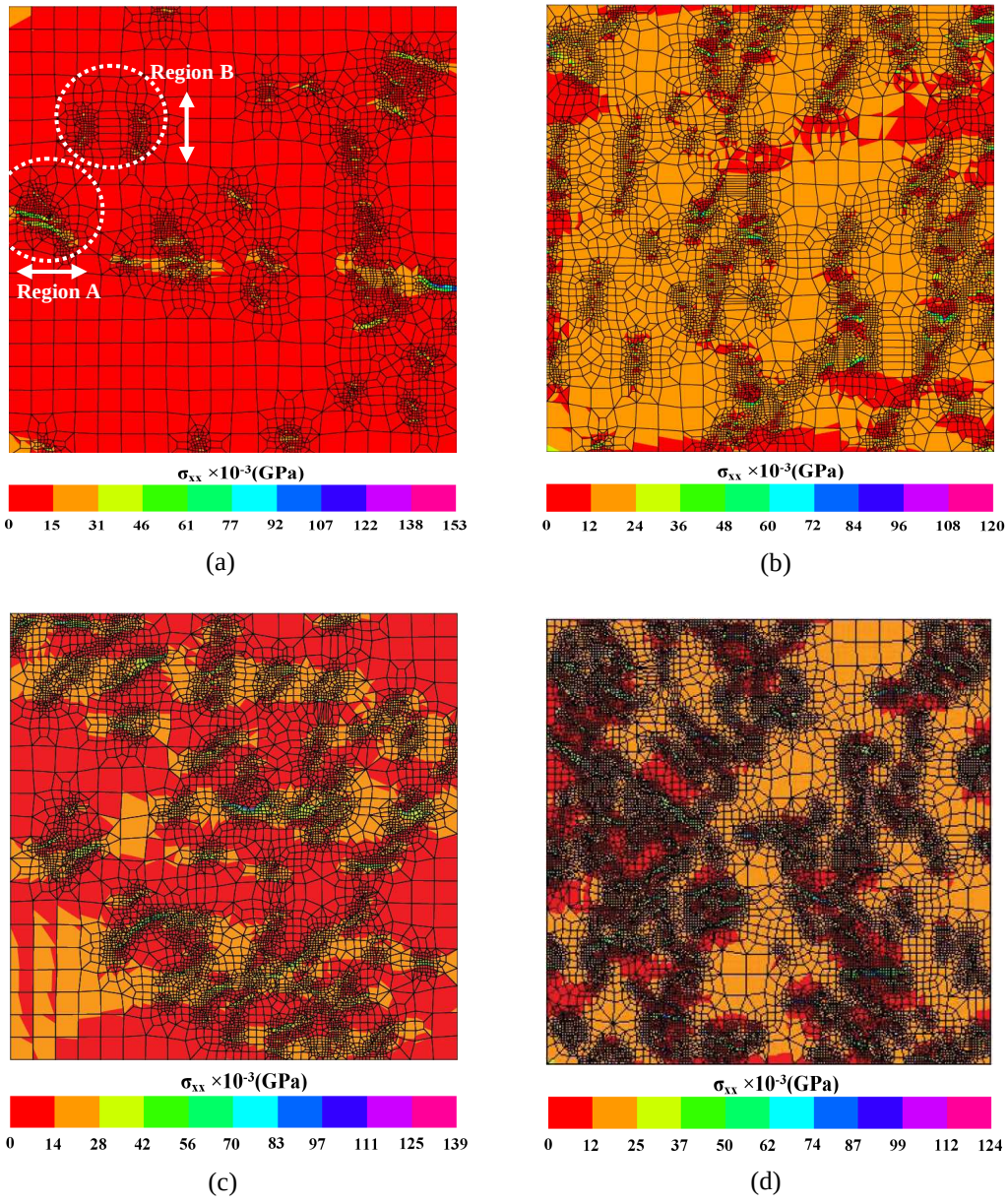

Fig. 7 Uniaxial stress (σ_{xx}) contours of optimised PP/clay nanocomposites (WR=2:1) with various clay contents (U_x =0.25% strain): (a) 3 wt%, (b) 5 wt%, (c) 8 wt% and (d) 10 wt%.

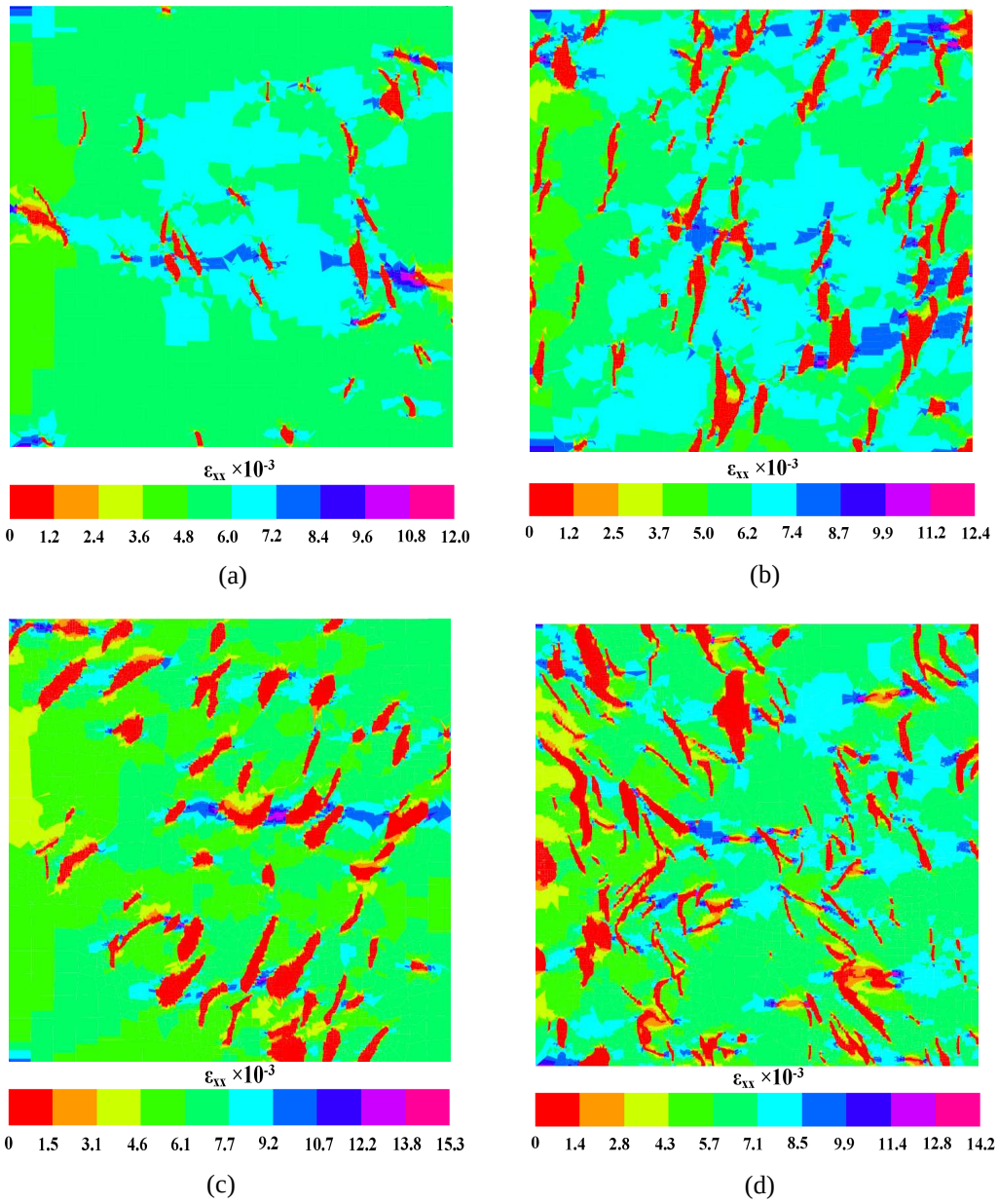

Fig. 8 Elastic strain (ε_{xx}) contours of optimised PP/clay nanocomposites (WR=2:1) with various clay contents (U_x =0.25% strain): (a) 3 wt%, (b) 5 wt%, (c) 8 wt% and (d) 10 wt%.

The corresponding elastic strain contours (ε_{xx}) for the local deformation behaviour are depicted in Fig. 8. Since rigid fillers like clay particles can naturally resist the deformation (i.e. straining) due to their high modulus, the elastic strains of all clay particles become relatively small compared to those of the PP matrix regardless of the clay content in such nanocomposites. PP matrix regions full of clay particles indicate the higher strains parallel to the loading direction. Apart from the clay intercalated structures, large particle size and close particle contact promote a greater deformation level within the PP matrix in the vicinity of clay particles, where the weak zones are developed leading to mechanical failure. Conversely, the particle-free PP matrix becomes less deformed and more inhomogeneous elastic strain distributions are clearly observed with increasing the clay content. In this study, OOF modelling results clearly show that the reasons for poor mechanical properties are often associated with the particle agglomeration for nanocomposites with higher clay contents. They also highlight the importance of properly processing nanocomposites and getting better clay particle distributions.

Conclusions

A comprehensive approach has been successfully developed to statistically determine the optimised material formulations of PP/clay nanocomposites leading to the significant property enhancement.

Taguchi design of experiments has been found to be very effective in the appropriate material selection and the suitability of manufacturing conditions. The novel OOF modelling technique provides the great insight to well predict the elastic moduli of PP/clay nanocomposites in comparison to conventional composites theoretical models and investigate the deformation mechanism of clay particles on the basis of mapping the real micro/nanostructures. As expected, the uniform clay dispersion is still a key issue from both experimental and numerical point of view as clay clusters can lead to the localised stress concentrations, thus making nanocomposites more prone to crack initiation.

Acknowledgements

Financial support for this study was provided by the Tertiary Education Commission (TEC), New Zealand and the Foundation for Research, Science and Technology (FRST), New Zealand under FRST grant #UOAX 0406. The authors also gratefully acknowledge Drs. Seung-Ill Haan and Stephen A. Langer (NIST, USA) for their kind technical support in OOF modelling.

References

[1] S.G. Lei, Formulation and mechanical properties of polypropylene nanocomposites, M.ASc thesis, Concordia University, Department of Mechanical and Industrial Engineering (2003).
[2] W. Lertwimolnun and B. Vergnes, Polymer, 46, 3462-71(2005).
[3] N. Hasegawa, M. Kawasumi, M. Kato, A. Usuki and A. Okada, J. Appl. Polym. Sci., 67, 87-92 (1998).
[4] X.H. Liu and Q.J. Wu, Polymer, 42, 10013-9 (2001).
[5] Y. Wang, F.B. Cheng and K.C. Wu, J. Appl. Polym. Sci., 93,100-12 (2004).
[6] D. Gicía-López, O. Picazo, J.C. Merino and J.M. Pastor, Eur. Polym. J., 39, 945-50 (2003).
[7] Y. Dong, D. Bhattacharyya and P.J. Hunter, Compos. Sci. Technol., in press, available online 30 October 2007.
[8] E.C. Lee, D.F. Mielewski and R.J. Baird, Polym. Eng. Sci., 44, 1773-82 (2004).
[9] X.H. Liu and Q.J. Wu, Polymer, 42, 10013-9 (2001).
[10] J.C. Halpin and J.L. Kardos, Polym. Eng. Sci., 16, 344-52 (1976).
[11] T. Mori and K. Tanaka, Acta. Metall., 21, 571-4 (1973).
[12] T.D. Fornes and D.R. Paul, Polymer, 44, 4993-5013 (2003).
[13] D.A. Brune and J. Bicerano, Polymer, 43, 369-87 (2002).
[14] N. Sheng, M.C. Boyce, D.M. Parks, G.C. Rutledge, J.I. Abes and R.E. Cohen, Polymer, 45, 487-506 (2004).
[15] J.J. Luo, I.M. Daniel, Compos. Sci. Technol. 63, 1607-16 (2003).
[16] E. Hackett, E. Manias and E.P. Giannelis, Chem. Mater. 12, 2161-7 (2000).
[17] G.M. Odegard, T.C. Clancy and T.S. Gates, Polymer, 46, 553-62 (2005).
[18] K.S. Katti, D. Sikdar, D.R. Katti, P. Ghosh and D. Verma, Polymer, 47, 403-14 (2006).
[19] M. Fermeglia and S. Pricl, Prog. Org. Coat., 58, 187-99 (2007).
[20] R. Toth, A. Coslanich, M. Ferrone, M. Fermeglia, S. Pricl, S. Miertus and E. Chiellini, Polymer, 45, 8075-83 (2004).
[21] M. Fermeglia, M. Ferrone and S. Pricl, Mol. Simul., 30, 289-300 (2004).
[22] R. Toth, M. Ferrone, S. Miertus, E. Chiellini, M. Fermeglia and S. Pricl, Biomacromolecules, 7, 1714-9 (2006).
[23] L.J. Zhu and K.A. Narh, J. Polym. Sci., 42, 2391-406 (2004).
[24] R.S. Fertig III and M.R. Garnich, Compos. Sci. Technol., 64, 2577-88 (2004).
[25] S.A. Langer, E.R. Fuller Jr. and W.C. Carter, Comput. Sci. Eng., 3, 15-23 (2001).
[26] S.A. Langer, A.C.E. Reid, S.I. Haan and R.E. Garcia**,** The OOF2 manual: Revision 3.7 for OOF2 Version 2.0.4, the National Institute of Standards and Technology (NIST), USA. [Online]: http://www.ctcms.nist.gov/~langer/oof2man/index.html
[27] N. Chawla, B.V. Patel, M. Koopman, K.K. Chawla, R. Saha, B.R. Patterson, E.R. Fuller and S.A. Langer, Mater. Charact., 49, 395-407 (2003).
[28] C.H. Hsueh, E.R. Fuller Jr., S.A. Langer and W.C. Carter, Mater. Sci. Eng. A, 268, 1-7 (1999).
[29] M.H. Zimmermann, D.M. Baskin, K.T. Faber, E.R. Fuller Jr., A.J. Allen and D.T. Keane, Acta Mater., 49, 3231-42 (2001).
[30] V. Cannillo, G.C. Pellacani, C. Leonelli, A.R. Boccaccini, Compos. Part A, 34, 43-51 (2003).
[31] V. Cannilo, C. Leonelli, T. Manfredini, M. Montorsi, P. Veronesi, E.J. Minay and A.R. Boccaccini, Compos. Sci. Technol., 65, 1276-83 (2005).

[32] V. Cannillo, T. Manfredini, M. Montorsi, C. Siligardi and A. Sola, J. Eur. Ceram. Soc., 26, 3067-73 (2006).
[33] V.R. Vedula, S.J. Glass, D.M. Saylor, G.S. Rohrer, W.C. Carter, S.A. Langer and E.R. Fuller, J. Am. Ceram. Soc., 84, 2947-54 (2001).
[34] V. Cannillo, C. Leonelli and A.R. Boccaccini, Mater. Sci. Eng. A, 323, 246-50 (2002).
[35] Z. Wang, A. Kulkarni, S. Deshpande, T. Nakamura and H. Herman, Acta. Mater., 51, 5319-34 (2003).
[36] V. Cannillo, F. Bondioli, L. Lusvarghi, M. Montorsi, M. Avella, M.E. Errico and M. Malinconico, Compos. Sci. Technol., 66, 1030-7 (2006).
[37] M. Avella, F. Bondioli, V. Cannillo, M.E. Errico, A.M. Ferrari, B. Focher, M. Malinconico, T. Manfredini and M. Montorsi, Mater. Sci. Technol., 20, 1340-4 (2004).
[38] F. Bondioli, V. Cannillo, E. Fabbri and M. Messori, J. Appli. Polym. Sci., 97, 2382-6 (2005).
[39] S.H. Park, Robust design and analysis for quality engineering, Chapman & Hall, London (1996).
[40] R.H. Lochner and J.E. Matar, Design for quality: an introduction to the best of Taguchi and western methods of statistical experimental design, Quality Resources and ASQC Quality Press, Milwaukee, WI (1990).
[41] X. Kornmann, H. Lindberg and L.A. Berglund, Polymer, 42, 1303-10 (2001).
[42] Y. Dong and D. Bhattacharyya, Compos. A, 39, 1177-91 (2008).
[43] Y. Dong, Multi-scale effects on deformation mechanisms of polymer nanocomposites: experimental characterisation and numerical study, PhD thesis, the University of Auckland, Department of Mechanical Engineering (2008).
[44] C.L. Tucker III and E. Liang, Compos. Sci. Technol., 59, 655-71(1999).
[45] C.Y. Hui and D. Shia, Polym. Eng. Sci., 38, 774-82 (1998).
[46] M. van Es, F. Xiqiao, J. van Turnhout and E. van der Giessen, Comparing polymer-clay nanocomposites with conventional composites using composite modelling. In: S. Al-Malaika, A.W. Golovoy, editors. Specialty polymer additives: principles and applications, Chapter 21, p 391-414, Blackwell Science, Oxford (2001).
[47] D. Hull and T.W. Clyne, An introduction to composite materials, 2nd ed., Cambridge University Press, New York (1996).
[48] D.H. Kim, P.D. Fasulo, W.R. Rodgers and D.R. Paul, Polymer, 48, 5308-23 (2007).
[49] X. Li, H. Gao, W.A. Scrivens, D. Fei, V. Thakur, M.A. Sutton, A.P. Reynolds and M.L. Myrick, Nanotechnology, 16, 2020-9 (2005).
[50]V. Mittal, J. Thermoplast. Compos. Mater., 20, 575-99 (2007).